Indentation in single crystals

Qiang Liu, Murat Demiral, Anish Roy, Vadim V. Silberschmidt
A.Roy3@lboro.ac.uk

Abstract

The process of indentation in three types of single crystals (FCC copper, BCC Ti-64 and Ti-15-3-3) was investigated using crystal-plasticity modelling. In order to investigate the effects of strain gradient on nanoindentation, both conventional single-crystal-plasticity and mechanism-based strain-gradient crystal-plasticity models were employed. For each type of single crystal, idealized conical and spherical indenters were incorporated into indentation simulations. The simulation results indicate that realization of indentation size effect was significantly affected by the indenter geometry and imposed strain gradient. Indentation hardness decreased with depth for a conical indenter but increased for a spherical one in the range of small indentation depths.

1 Introduction

Modelling of micro-/nano-indentation of single crystals has been developed extensively to elucidate experimentally observed features such as the size effect, pile-up phenomenon and lattice rotations. For instance, Liu et al. [1] performed crystal-plasticity (CP) finite-element (FE) numerical simulations and micro-indentation experiments to determine mechanical properties of single-crystal copper. Lee and Chen [2] adopted a mechanism-based strain-gradient crystal-plasticity (MSGCP) theory to model the size effect in micro-indentation in the same material. Wang et al. [3] studied an effect of crystallographic orientation on pile-up patterns and micro-textures using a CP FE model for single-crystal copper. Correct numerical predictions of the surface pile-up patterns were achieved; however, a difference of an order of a magnitude in the load-displacement curve between experiments and simulations was reported. Liu et al. [1] performed a similar study using a spherical indenter instead of a conical one, where satisfactory agreements between the numerical and experimental load-displacement curves were demonstrated. However, different magnitudes of a coefficient of friction were used to represent a contact condition between the indenters tip and the workpiece material for different orientations to match numerically obtained surface profiles with the experimental data. An error of up to 50% was reported for a magnitude of the maximal pile-up. In the study of Demiral et al. [4], where both the incipient and evolving strain gradients were considered in the calibration procedure (unlike prior studies), a better agreement for the load-displacement curves and maximum pile-up heights was obtained. Zahedi et al. [5][6] studied the effects of crystal orientation on a cutting force and chip

morphology in metal machining, where the continuum CP FE method was combined with smoothed particle hydrodynamics to overcome the problem of element distortion in CP FE simulations.

Some numerical studies have attempted to analyse physical deformation mechanisms leading to lattice rotations. For instance, Wang et al. [3] demonstrated lattice rotations for a single crystal of Cu with different orientations using a 3D elastic viscoplastic CP FE technique. Zaafarani et al. [7] proposed a physically based CP model based on dislocation-rate formulations to explain potential reasons for deformation-induced patterns consisting of multiple narrow zones with alternating crystalline rotations. However, the model consistently overestimated the extent of lattice rotations in the experiment. Demiral et al. [8] developed a 3D FE model of nano-indentation incorporating an enhanced model of the strain-gradient crystal plasticity [9] to simulate accurately deformation of a body-centred cubic metallic material. It was noted that deformation-induced lattice rotations can be predicted correctly using the strain-gradient CP theory since the effect of GNDs was accounted for (via strain gradients). This study demonstrated that the introduction of strain gradients altered the activity of slip systems and the relative contribution to the overall plastic slip.

2 Model

In this part, the indentation size effect(ISE) of three types of single crystals, namely, FCC copper, BCC β phase of Ti-6Al-4V (β-Ti-64) and BCC β phase of Ti-15V-3Cr-3Al-3Sn (β-Ti-15-3-3-3), was investigated using crystal-plasticity models. In indentation modelling, idealised conical and spherical indenters were chosen to study the effects of indenter's geometry on the mechanical response of the tested material. The chosen half-angle of the conical indenter was 72° and the radius of spherical indenter $2.5\mu m$; dimensions of the modelled work-piece were $(16 \times 16 \times 8)\mu m^3$. The top surface of the modelled workpiece was free of constraints and normal displacements of all the other faces were fixed. Friction between the indenter and the indented surface was ignored for simplicity. The maximum indentation depths for all simulations was $h_{max} = 0.5\mu m$.

A crystal plasticity model was used to describe the material's behaviour of these single crystals during nanoindentation. It is well known that conventional CP models do not account for the deformation mechanism at the smallest length-scale accurately as they do not consider dislocation evolution and propagation explicitly. In our study, a conventional single-crystal plasticity (SCP) model [10] and the MSGCP model [11] were employed to compare and contrast the (de)merits of the two models. Both models had a similar constitutive framework, with the latter accounting for the effect of strain-gradients. The relationship between the shear rate $\dot{\gamma}^{(\alpha)}$ and resolved shear stress $\tau^{(\alpha)}$ on the slip system α is expressed by the power law proposed by Hutchinson [12], as

$$\dot{\gamma}^{(\alpha)} = \dot{\gamma}_0 |\frac{\tau^\alpha}{g^\alpha}|^n sgn(\tau^\alpha) \tag{1}$$

where $\dot{\gamma}_0$ is the reference shear rate, $g^{(\alpha)}$ is the slip resistance and n is the rate-

sensitivity parameter. The evolution of $g^{(\alpha)}$ is given by

$$\dot{g}^{(\alpha)} = \sum_{i=1}^{n} h_{\alpha\beta}|\dot{\gamma}^{(\beta)}| \tag{2}$$

where $h_{\alpha\beta}$ is the hardening modulus that is calculated from the relation propose by Hutchinson [12]:

$$h_{\alpha\alpha} = h_0 \mathrm{sech}^2(\frac{h_0\gamma}{\tau_s - \tau_0}), h_{\alpha\beta} = q h_{\alpha\alpha}(\alpha \neq \beta), \gamma = \sum_{\alpha}\int_0^t |\dot{\gamma}^{(\alpha)}|dt. \tag{3}$$

Here, h_0 is the initial hardening modulus, q is the latent hardening ratio, τ_0 and τ_s are the shear stresses at the onset of yield and the saturation of hardening, respectively. The accumulative shear strain over all the slip systems is represented by γ. Generally, τ_0 is equal to the value of initial slip resistance $\tau_0 = g^{(\alpha)}|_{(t=0)} = g_0$.

The sole difference between SCP and MSGCP is the calculation of the slip resistance $g^{(\alpha)}$. In the SCP model, $g^{(\alpha)}$ was only determined by SSDs. In contrast, the contribution of GNDs was also taken into account in the MSGCP model, and $g^{(\alpha)}$ was redefined as

$$g_T^{(\alpha)} = \sqrt{(g_{SSD}^{(\alpha}})^2 + (g_{GND}^{(\alpha}})^2, \tag{4}$$

where, $g_{SSD}^{(\alpha)}$ and $g_{GND}^{(\alpha)}$ are contributions to the slip resistance caused by SSDs and GNDs, respectively. The evolution of slip resistance $g_{SSD}^{(\alpha)}$ was given by a strain-hardening equation:

$$\dot{g}_{SSD}^{(\alpha)} = \sum_{i=1}^{n} h_{\alpha\beta}|\dot{\gamma}^{(\beta)}| \tag{5}$$

The slip resistance $g_{GND}^{(\alpha)}$ was determined by the effective density of GNDs :

$$g_{GND}^{(\alpha)} = \alpha\mu\sqrt{b\eta_G^{(\alpha)}} \tag{6}$$

$$\eta_G^{(\alpha)} = |\mathbf{m}^{(\alpha)} \times \sum_{\beta}(s^{\alpha\beta} \bigtriangledown \gamma^{(\alpha)}) \times \mathbf{m}^{(\beta)}|. \tag{7}$$

In equation (6), b and μ are the Burgers vector and shear modulus, respectively. In equation (7), $\mathbf{m}^{(\alpha)}$ is the normal unit vector of slip plane, $s^{(\alpha)}$ and $s^{(\beta)}$ define the slip direction. Consequently, the MSGCP model could be reduced to the SCP model if $g^{(\alpha)} = g_T^{(\alpha)} = g_{SSD}^{(\alpha)}$.

The two types of crystal-plasticity models were implemented in the commercial FE code ABAQUS/Standard by using the user interface subroutine, UMAT. Calculation of a strain gradient in the MSGCP model was realized with the use of C3D8 element available in the FE package. The simulation results were reported in the form of hardness-indentation depth curves. Hardness H was defined as

$$H = \frac{F_{max}}{A}, \tag{8}$$

where F_{max} was the maximum load applied in indentation and A was the projected area of contact between the indenter and the work-piece. The contact area was determined by accounting for the contact nodes on the surface of the work-piece as outlined in the work of Lee and Chen [2]. To capture an accurate description of the contact area, a finer local mesh was used in regions underneath the indenter tip.

3 Results and Discussions

3.1 Indentation of FCC copper single crystal

The material parameters used in the work of Lee and Chen [2] was adopted for copper single crystal. The magnitude of Burgers vector for copper is $b = 0.255nm$, shear modulus $\mu = 42.0GPa$ and the empirical coefficient in the Taylor model is $\alpha = 0.5$. For the investigated FCC copper single crystal, the slip was assumed to occur on the usual twelve $\{111\}\langle 110\rangle$ slip systems. For both conical and spherical indenters, the indentation simulations were performed on the crystallographic plane of the work-piece.

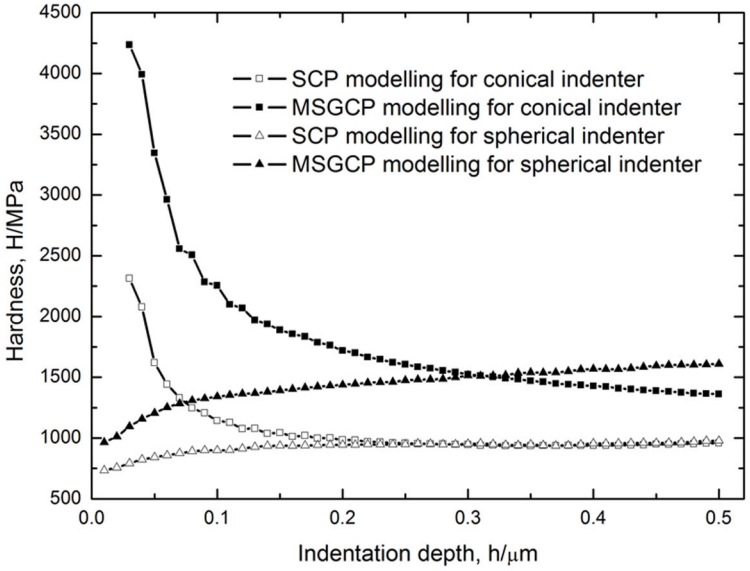

Figure 1: Indentation size effect for copper single crystal for conical and spherical indenters

Variations of hardness with indentation depth in nanoindentation with conical and spherical indenters are presented in Figure 1. ISE was clearly observed for the two types of indenter, although the hardness-indentation depth curves for the spherical indenter exhibited lower depth sensitivity. Interestingly, the trend of the change in hardness with indentation depth was different for conical and spherical indenters. We observed that the reported hardness reduce with increasing depth for the conical indenter, however, the trend was opposite for the spherical one. Therefore, the indenter geometry not only affected the magnitude of calculated

hardness but also the nature of ISE. Our study demonstrated that the difference in hardness related to indenter geometry was more significant at lower indentation depths.

For the two types of indenters, it was clear that predictions based on the MSGCP model were significantly different from those with the SCP model, as shown in Figure 1. This implies that strain gradients played a pivotal role in defining hardness (and overall deformation). It also infers that strain gradient lead to an increase in hardness at smaller indentation depths for the conical indenter; however, the tendency was reversed for the spherical indenter. For the simulation results based on SCP modelling, it was noted that the hardness became insensitive to the depth when the indentation depth exceeded 0.2 μm. This phenomenon was different for MSGCP modelling. A gradual decrease or increase of hardness with higher indentation depth was observed for conical and spherical indentations, respectively. Therefore, the effect of indenter geometry on hardness was observed even at a large indentation depth due to the effect of strain gradients.

3.2 Indentation of BCC Ti-64 single crystal

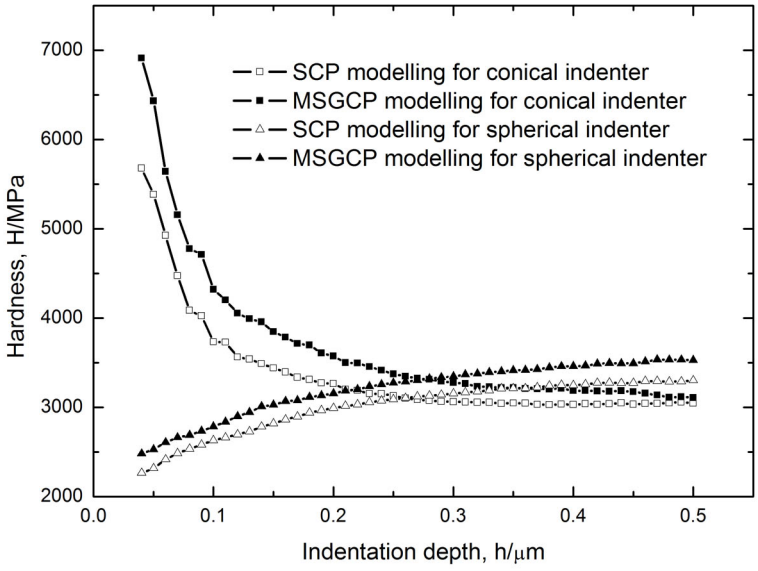

Figure 2: Indentation size effect for copper single crystal for conical and spherical indenters

Material parameters used for modelling the BCC β-Ti-64 single crystal were cited in literature [13][14]. The magnitude of Burgers vector $b = 0.286nm$, the shear modulus $\mu = 42.085GPa$ [15] and $\alpha = 0.5$ were chosen based on prior studies. Twelve $\{110\}\langle 111\rangle$ slip systems were considered for β-Ti-64. For both conical and spherical indenters, the simulations were performed on the [110] crystallographic plane.

In Figure 2, the variations of hardness with indentation depth are shown demonstrating a significant ISE. For both SCP and MSGCP simulation results, there was

an evident discrepancy in hardness caused by the indenter geometry. At a small indentation depth, the hardness obtained for the conical indenter was larger than that for the spherical one; however, a higher hardness was observed for the spherical indenter at large indentation depths. It is important to point out that the discrepancy in hardness between the two types of indenters existed even if the effect of strain gradients was neglected. Note that Ti-64 has a much higher slip resistance than Cu. For the range of indentation depths studied, the proportion of plasticity to elasticity in the contact area of Cu is larger than that in Ti-64. Thus, an increase in hardness was observed when using the spherical indenter due to its propensity to induce elastic deformation. At each indentation depth, the strain-gradient effect was small.

3.3 Indentation of BCC Ti-15-3-3 single crystal

Material parameters of a BCC β-Ti-15-3-3 single crystal were obtained by calibrating experimental results in our previous work [4]. Here, twelve $\{112\}\langle 111\rangle$ were taken as the dominant the slip systems. For both conical and spherical indenters, the indentation simulations were performed on the [110] crystallographic plane of the material.

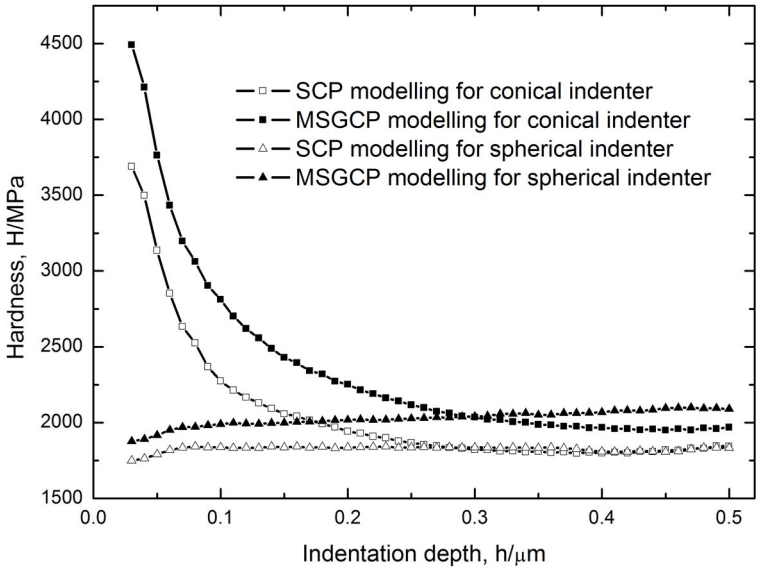

Figure 3: Indentation size effect for copper single crystal for conical and spherical indenters

The ISE in Ti-15-3-3 is shown in Figure 3. The hardness magnitudes obtained for the conical indenter exhibit a significant depth-dependence in comparison to those for the spherical indenter. For the SCP model, the effect of indenter geometry on hardness was considerable when the indentation depth was smaller than 0.25 μm but could be neglected at larger depths, similar to the results for the FCC Cu single crystal (Figure 1). In contrast, the results from the MSGCP model indicate that

a difference in hardness for the two types of indenters exists, but is less significant than that for BCC Ti-64 (Figure 2).

4 Conclusions

The ISE was observed for nanoindentation of the three investigated single crystals for both conical and spherical indenters at small indentation depth. The indenter geometry had a significant effect on the features of ISE: the calculated hardness magnitude decreased with the indentation depth for the conical indenter but increased for the spherical one. Therefore, a great discrepancy in hardness for different types of indenters was observed, especially when the indentation depth was relatively small. However, hardness became less sensitive to the depth at larger indentation depths. For all the three types of single crystals studied, the variation of hardness with indentation depth was higher for the conical indenter. In these monocrystals, strain gradients played different roles in nanoindentation. It is emphasized that both the effects of indenter geometry and strain gradients were related to each other. The difference in hardness caused by the indenter geometry could be neglected when the effects of strain gradients were not considered for metal single crystals with low slip resistance (FCC copper and BCC Ti-15-3-3 single crystals). The indenter geometry also influenced strain gradients that, in turn, affected hardness. The discrepancy in hardness between the results of MSGCP and SCP models decreased with indentation depth for the conical indenter but the trend was opposite for the spherical indenter. The presented simulation results indicate that there are several geometrical and mechanical factors, which affect the data obtained with nanoindentation of single crystals. The modelling approach such as described here helps to elucidate the mechanisms that lead to deformation in the small scale.

5 Acknowledgement

Funding from the Engineering and Physical Sciences Research Council (UK) through grant EP/K028316/1 and Department of Science and Technology (India), project MAST, is gratefully acknowledged.

References

[1] Y Liu, S Varghese, J Ma, M Yoshino, H Lu, and R Komanduri. Orientation effects in nanoindentation of single crystal copper. International Journal of Plasticity, 24(11):19902015, 2008.

[2] WB Lee and YP Chen. Simulation of micro-indentation hardness of FCC single crystals by mechanism-based strain gradient crystal plasticity. International Journal of Plasticity, 26(10):15271540, 2010.

[3] Y Wang, D Raabe, C Kluüber, and F Roters. Orientation dependence of nanoindentation pile-up patterns and of nanoindentation microtextures in copper single crystals. Acta Materialia, 52(8):22292238, 2004.

[4] M Demiral, A Roy, and VV Silberschmidt. Indentation studies in bcc crystals with enhanced model of strain-gradient crystal plasticity. Computational Materials Science, 79:896902, 2013.

[5] A Zahedi, S Li, A Roy, V Babitsky, and VV Silberschmidt. Application of smooth-particle hydrodynamics in metal machining. In Journal of Physics: Conference Series, 382, 012017. 2012.

[6] SA Zahedi, M Demiral, A Roy, and VV Silberschmidt. FE/SPH modelling of orthogonal micro-machining of FCC single crystal. Computational Materials Science, 78:104-109, 2013.

[7] N Zaafarani, D Raabe, F Roters, and S Zaefferer. On the origin of deformation induced rotation patterns below nanoindents. Acta Materialia, 56(1):3142, 2008.

[8] M Demiral, A Roy, T El Sayed, and VV Silberschmidt. Influence of strain gradients on lattice rotation in nano-indentation experiments: A numerical study. Materials Science and Engineering: A, 608:7381, 2014.

[9] M Demiral. Enhanced gradient crystal-plasticity study of size effects in bcc metal. PhD thesis, Loughborough University, 2012.

[10] Y Huang. A User-material Subroutine Incroporating Single Crystal Plasticity in the ABAQUS Finite Element Program. Harvard Univ., 1991.

[11] C-S Han, H Gao, Y Huang, and W D Nix. Mechanism-based strain gradient crystal plasticity-I. theory. Journal of the Mechanics and Physics of Solids, 53(5):1188-1203, 2005.

[12] JW Hutchinson. Bounds and self-consistent estimates for creep of polycrystalline materials. Proceedings of the Royal Society of London. Series A, Mathematical and Physical Sciences, 101-127, 1976.

[13] AC Lewis, SM Qidwai, and AB Geltmacher. Slip systems and initiation of plasticity in a body-centered-cubic titanium alloy. Metallurgical and Materials Transactions A, 41(10):25222531, 2010.

[14] J Thomas, M Groeber, and S Ghosh. Image-based crystal plasticity FE framework for microstructure dependent properties of Ti–6Al–4V alloys. Materials Science and Engineering: A, 553:164175, 2012.

[15] XG Fan and He Yang. Internal-state-variable based self-consistent constitutive modeling for hot working of two-phase titanium alloys coupling microstructure evolution. International Journal of Plasticity, 27(11):18331852, 2011.

Qiang Liu, Wolfson School of Mechanical and Manufacturing Engineering, Loughborough University, LE11 3TU, UK

Murat Demiral, Department of Mechanical Engineering, University of Turkish Aeronautical Association, Ankara, Turkey, 06790

Anish Roy, Wolfson School of Mechanical and Manufacturing Engineering, Loughborough University, LE11 3TU, UK

Vadim V. Silberschmidt, Wolfson School of Mechanical and Manufacturing Engineering, Loughborough University, LE11 3TU, UK